Ion Exchange Lithography: Localized Ion Exchange Reactions for Spatial Patterning of Perovskite Semiconductors and Insulators

*Lukas Helmbrecht, Moritz H. Futscher, Loreta A. Muscarella, Bruno Ehrler, Willem L. Noorduin**

Dr. L. H., Dr. M. H. F., L. A. M., Prof. B. E., Dr. W. L. N.
AMOLF, Science Park 104, 1098 XG Amsterdam, The Netherlands.
E-mail: noorduin@amolf.nl

Keywords: ion exchange, perovskite, ion exchange lithography

Patterning materials with different properties in a single film is a fundamental challenge and essential for the development of next-generation (opto)electronic functional components. This work introduces the concept of ion exchange lithography and demonstrates spatially controlled patterning of electrically insulating films and semiconductors with tunable optoelectronic properties. In ion exchange lithography, a reactive nanoparticle “canvas” is locally converted by printing ion exchange “inks”. To demonstrate the proof of principle, a canvas of insulating nanoporous lead carbonate is spatioselectively converted into semiconducting lead halide perovskites by contact printing an ion exchange precursor ink of methylammonium and formamidinium halides. By selecting the composition of the ink, the photoluminescence wavelength of the perovskite semiconductors is tunable over the entire visible spectrum. A broad palette of conversion inks can be applied on the reactive film by printing with customizable stamp designs, spray-painting with stencils, and painting with a brush to inscribe well-defined patterns with tunable optoelectronic properties in the same canvas. Moreover, the optoelectronic properties of the converted canvas are exploited to fabricate a green light-emitting diode (LED), demonstrating the functionality potential of ion exchange lithography.

1. Introduction

Spatial arrangement of materials with contrasting properties is fundamentally interesting and essential for integrated (opto)electronic devices.[1,2] Nanoparticles are versatile building blocks for achieving such arrangement by both bottom-up and top-down assembly.[2-22] Spatial patterning of nanoparticles has been achieved by methods such as patchy particles, oriented attachment, hierarchical self-assembly, topological templates, and optical and e-beam lithography .[2–16,23] Moreover, the entire ensemble of nanoparticles can be converted into a desirable chemical composition using ion exchange reactions, while preserving the pattern of the ensemble.[4,17–22] Also, selected areas of the ensemble can first be encapsulated with a passivating coating, after which only the uncoated nanoparticles undergo conversion during ion exchange.[24] Hence, organization of different composition is possible in many ways, but often requires multiple steps to achieve control over patterning and chemical composition, making the overall process difficult and expensive.[2,16]

Locally applying the reagents offers an alternative approach for spatial arrangement of materials with desirable properties. For thousands of years, printing of inks on canvases has spurred human development. Recently, methods such as microcontact printing have been used extensively to locally functionalize substrates and infuse reactants in gels.[25–28] Inspired by these works, we here introduce the concept of ion exchange lithography (IEL). We show that spatial patterning of materials can simply be achieved by printing ion exchange “inks” on a reactive nanoparticle “canvas”. Importantly, to act as a versatile canvas, the nanoparticle film should enable ion exchange to many different chemical compositions. The ink, on the other hand, should react the contacted area of the canvas to one specific composition only, while other reaction products ideally leave the canvas automatically.

To demonstrate the proof-of-principle of IEL, we explore the spatially controlled conversion of an electrically insulating canvas into semiconducting lead halide perovskites. The extraordinary properties of perovskites, in combination with their simple synthesis, is revolutionizing the field of optoelectronics.[29–31] Spatially organizing perovskites alongside materials with fundamentally different properties is essential for integrated devices such as displays, detectors, and scintillators.[32–37] Spatial positioning of perovskites has been achieved using, for instance, photolithography, laser writing, templates, nanoimprint lithography, and inkjet printing,[38–47] and post synthesis modification of perovskites has enabled local modification of the light emission color.[48,49] Nevertheless, such approaches are often laborious and slow, and require specialized equipment, thus making them difficult to scale up. This highlights the need for new strategies to directly achieve spatial organization of desirable compositions in a simple and scalable manner.

Here we integrate semiconducting perovskites in an electrically insulating film by printing, painting, and spraying reactive inks on an ion exchange reactive canvas. Note that while the previously developed techniques achieve patterns though depositing, removing, or shaping perovskite, we here convert an insulating film into perovskite. The versatility of this IEL approach allows for scalability and arbitrary, user-defined patterns. The photoluminescence wavelength of the perovskite semiconductors is tunable over the entire visible spectrum by selecting the composition of the ink. Moreover, we show that the IEL approach can be integrated into the fabrication of (opto)electronic devices such as light-emitting diodes (LED).

2. Results and Discussion

Our approach is illustrated in **Figure 1**. In short, nanoscopic lead carbonate ($PbCO_3$) crystals are deposited in a thin film. This electronically insulating lead carbonate ($PbCO_3$) film acts as reactive canvas, while a solution of methylammonium halides (CH_3NH_3X or MAX; X = Cl, Br,

or I) is the reactive ink. Contact printing of the ink on the canvas results in the local conversion of $PbCO_3$ into semiconducting methylammonium lead halide perovskites ($CH_3NH_3PbX_3$ or $MAPbX_3$; X = Cl, Br, or I) following the previously developed reaction:[21]

$$PbCO_3\ (s) + 3\ CH_3NH_3X\ (l) \rightleftarrows H_2O\ (l) + CO_2\ (g) + 2\ CH_3NH_2\ (g) + CH_3NH_3PbX_3\ (s) \quad (1).$$

The acidic pH facilitates the replacement of carbonate for the halide anion, followed by insertion of the methylammonium halide to rearrange the crystal structure into the perovskite. This reaction is ideal for testing our approach: the $PbCO_3$ is insoluble and thus suitable for acting as the reactive canvas, while CH_3NH_3X can be dissolved in common solvents such as isopropyl alcohol (IPA) and therefore act as the ink.[50] Moreover, the $PbCO_3$ canvas can react into perovskites with different chemical compositions, where the choice of the CH_3NH_3X ink will determine the exact composition of the perovskite that forms in the canvas. The solvent, as well as the other reaction products, H_2O, CO_2, and CH_3NH_2 simply evaporate from the film, thus driving the reaction from $PbCO_3$ to perovskite.

To demonstrate the proof-of-principle, we fabricate nanoporous films by drop casting nanoscopic $PbCO_3$ crystals onto glass substrates (see Supporting Information, SI for details). High-resolution Scanning Electron Microscopy (SEM) shows that the particles have typical sizes between 40 and 300 nm, and are densely packed into uniform films while still exhibiting nanoscale porosity **(Figure 2a)**. We find that the film thickness can be tuned between ca. 0.25-5.0 μm by controlling the drop casting conditions (Figure 2 and SI).

We perform the ion exchange contact printing by bringing the $PbCO_3$ film in contact with a solution of MAX in anhydrous isopropyl alcohol (IPA). IPA was selected as solvent based on the following criteria: (1) The solvent should dissolve the precursors MAX and FAX, while (2) not dissolving the perovskite (hence disqualifying solvents such as DMSO and DMF). (3) The

vapor pressure should be sufficiently high to enable full evaporation. (4) The solvent should enable partial wetting of the film by capillary forces. The conversion ink is applied using customized silicone and polydimethylsiloxane (PDMS) stamps (see SI). These materials are easily moldable and chemically inert. In addition, the hardness of these materials can be tuned to achieve uniform contact between the film and the stamp while keeping the canvas intact (see SI).[25,27]

The local conversion is demonstrated by applying MABr-IPA on the $PbCO_3$ canvas using a stamp patterned with rectangular pillars. Within seconds the white $PbCO_3$ transforms into yellow-orange perovskite at the points of contact with the stamp, thereby meticulously replicating the pattern of the stamp with high fidelity (See SI for comparison of a stamp and stamped pattern). Moreover, IR-spectroscopy confirms the absence of side products on the converted film (see SI).

The optoelectronic properties of the converted pattern can directly be visualized by exciting the electronic structure with an ultra-violet (UV) light source (Figure 2d). We observe bright green photoluminescence (PL) from the converted rectangles, whereas the lead carbonate in the pristine part of the film did not convert to the perovskite and therefore did not emit any light. Photoluminescence spectroscopy showed that the emission wavelength of the converted pattern peaked at 530 nm, which is consistent with previous PL measurements of $MAPbBr_3$.[21]

We explore the scalability of the pattern dimensions. For most practical applications, feature sizes on the order of 100 µm are required (e.g. 150 µm pixel size in a 13” full HD display). We use a high-resolution PDMS stamp with a height of 10 µm and a diameter of 20 µm pillars that are spaced 100 µm apart. Again, the pattern is faithfully replicated into an array of perovskite dots (Figure 2b). We investigate the resolution limits by comparing the stamp with the resulting

pattern. Deliberate overwetting the stamp results in broadening of the pattern, suggesting lateral spreading within the film due to capillary forces. Optimizing the amount of applied ink allows minute replication of the PDMS stamp into a pattern with only slight size variations of 1-2 µm (Figure 2c). While capillary forces and ink volume currently limit the resolution, the ink is sufficiently wetting the film for the conversion reaction to occur while preserving the pattern.

The observed lateral spreading suggests that capillary forces will transport the ink also vertically into the depth of the film, thus enabling conversion throughout the canvas. Indeed, energy-dispersive X-ray spectroscopy (EDS) on a cross-sectioned sample reveals the presence of bromide throughout the depth of the canvas (Figure S3). Combined with fluorescence photographs of the backside of the opaque canvas, this indicates conversion from the top to the bottom (see SI, Figure S2). In the lateral direction at the edge of the wetted area, a well-defined boundary between the converted and unconverted area is achieved, according to EDS (Figure 2a). Although the grains undergo conversion to perovskite, the nanoscopic morphology is conserved, as observed via high-resolution electron microscopy (Figure 2a). Moreover, films with only 3.5 at% bromide (as compared to lead) already show bright emission, although the conversion can be increased to 25 at.% by prolonging the reaction time, whereas SEM analysis confirmed that the morphology of the particles remains preserved (see SI).

Reaction scheme 1 suggests that perovskites with different halide moieties—and therefore different emission colors—can be synthesized in the $PbCO_3$ film by selecting the corresponding methylammonium halide precursor in the ink. Indeed, mixing MAI into the MABr/IPA conversion ink yielded mixed-halide perovskite patterns with red PL, while MACl addition resulted in blue PL (Figure 2d). The emission wavelength can be tuned by the mixing ratios of different methylammonium halides in the conversion ink: e.g., 6:4 molar ratio MACl:MABr/IPA resulting in bright emission around 465 nm (Figure 2e), whereas 8:2 molar

ratio MAI:MABr yields deep red emission around 705 nm (Figure 2e). Hence, the color of the light-emitting patterns can be tuned over the whole visible spectrum.

IEL can be extended to other classes of perovskites. Formamidinium halide perovskites ($CH(NH_2)_2PbX_3$ or $FAPbX_3$) are of interest because of their greater chemical stability and longer carrier diffusion length while exhibiting comparable optical performance to methylammonium perovskites.[51,52] Conversion of $PbCO_3$ to $FAPbX_3$ is achieved using formamidinium halides instead of methylammonium halides in the precursor ink. Akin to MAX (reaction scheme 1), FAX can partly dissociate to form acid and thereby drive the exchange of carbonate with the halide group. Moreover, the chemical similarities between MAX and FAX as well as the structural similarities between the crystal lattices of $MAPbX_3$ and $FAPbX_3$ suggest an equivalent reaction pathway. The resulting $FAPbX_3$ perovskite patterns show bright luminescence with tunable PL emission throughout the visible spectrum by selecting the halide moiety between chloride, bromide, and iodide (Figure S4).

Based on these insights, we integrate perovskites with different emission wavelengths into a single canvas. To this aim, we sequentially print the ion mixtures for different perovskites on the lead carbonate film. Accurate spatial positioning of the different stamps is achieved by a guiding framework (see SI). To demonstrate the principle, we integrate rectangles of red, green, and blue-emitting semiconductors within the non-luminescent insulator to produce an array pattern akin to the ones commonly used in LED displays **(Figure 3a)**.

The ion exchange inks could be applied using many other traditional and scalable inking techniques such as inkjet-, offset-, and roll-to-roll printing. From this extensive repertoire, we test traditional artist's paintbrushes and an airbrush gun. With the paintbrush, freeform patterns can be achieved straightforwardly (Figure 3b). With the airbrush, large uniform areas can be

converted. Moreover, highly complex patterns can be achieved using laser-cut stencils as a shadow mask, which we exploit for creating a green luminescent portrait of Marie Skłodowska-Curie. (Figure 3c, Movie 1 in SI). An additional advantage of airbrushing is that this method is fast and contact-free while easily converting sizeable areas, hence averting the risk of damaging the film and offering compatibility for large-scale fabrication.

IEL offers exciting opportunities for the direct integration of materials with different electronic properties in functional devices. The converted $MAPbBr_3$ and $FAPbBr_3$ films show good photoluminescence quantum yields (PLQY) of 25±3 % and 40±5 % respectively, making them promising candidates for optoelectronic components. We explore this potential by fabricating an LED with $FAPbBr_3$ as the active layer (see **Figure 4a,b** and SI), and comparing this LED to a device based on a conventional spin coated $FAPbBr_3$ film with an identical layer stack. We characterize both devices by recording the current-voltage (IV) curves as well as measuring electroluminescence (EL). As expected for $FAPbBr_3$ LEDs, the IV curves display typical diode characteristics (Figure 4c). The ion exchange-based device exhibits a higher turn-on voltage indicating an increased resistance, likely due to the partially insulating nanoparticle interior of the film. Nevertheless, with applied voltage, the device operates as an LED and emits green EL around 540 nm as previously reported (Figure 4d),[53,54] While the performance may be further optimized by improving the connectivity between the particles themselves as well as with the electrodes, this proof-of-concept device already demonstrates the potential of IEL for functional (opto)electronic devices.

3. Conclusion

In conclusion, we here demonstrate spatially-controlled ion exchange reactions of lead carbonate films into lead halide perovskites. We show that this ion exchange-lithography method offers a simple, scalable, versatile, and highly customizable method for integrating

desirable complementary electronic and optoelectronic properties in arbitrary patterns that can be integrated into functional devices. Effectively, the conversion liquid and film can be regarded as reactive ink and canvas for integrating unusual and attractive properties with micrometer spatial control.

Semiconductors and lead carbonates have a long history in painting and other arts. Basic lead carbonate is one of the oldest synthetic pigments known, while semiconducting salts such cadmium sulfide and lead chromate enabled bright colors and were widely adopted by painters such as Monet and Van Gogh.[55–58] Traditionally, artists apply the semiconductors as pigment on the canvas. In contrast, our work enables conversion of the canvas into a semiconductor by painting a reactive ink.

Currently, the resolution of the patterns is mainly determined by: (1) properties of the ink (e.g. viscosity, volatility, polarity, wetting behavior), (2) the applied volume of ink, (3) properties of the film (e.g. porosity, particle size, surface chemistry etc.), and (4) the thickness of the film. The capillary forces are determined by the combined properties of the ink and the film, and balancing their contributions enables optimization of the resolution. Since the resolution of the converted patterns is to a large extent defined by the precision with which the conversion ink is applied, state-of-the-art technologies such as roll-to-roll and inkjet printing can be exploited. Moreover, photo-induced ion exchange reactions may offer opportunities for further improving the resolution with spatially-controlled light patterns.

Already, many ion exchange reactions have been developed in liquids.[17–21] We therefore envisage that the palette of conversion inks for our IEL methodology can straightforwardly be extended to a wide range of chemical compositions with desirable and unusual properties. In

addition, we foresee that nanocomposites could serve as attractive conversion canvases due to their outstanding mechanical properties and chemical reactivity.[21,59–61] Consequently, IEL may offer an attractive route for the synthesis of functional integrated devices such as displays and detectors that require complicated spatial patterning of complementary properties in a single film. Therefore, exciting opportunities will arise from expanding the microelectronic paint box, adding conversion inks for the synthesis of other semiconductors, transport layers, and conductors, which ultimately enables fully printed devices with ion exchange lithography.

Supporting Information
Supporting Information is available from the Wiley Online Library or from the author.

Acknowledgements
We thank Dion Ursem for designing and fabricating the stamp and guiding system. We thank Christiaan van Campenhout for assistance in creating the portrait of Marie Skłodowska-Curie and Marloes H. Bistervels for help in creating the "perovskite" lettering in Figure 3b. We thank Jian-Yao Zheng for assistance with the PLQY measurements. We thank Christiaan van Campenhout and Alexander Korotkevich for their assistance with the FTIR measurements. This work is part of the Vernieuwingsimpuls Vidi research program "Shaping up materials" with project number 016.Vidi.189.083, which is partly financed by the Dutch Research Council (NWO). The work of L.A.M. is part of the Vidi research program 016.Vidi.179.005.

Received: ((will be filled in by the editorial staff))
Revised: ((will be filled in by the editorial staff))
Published online: ((will be filled in by the editorial staff))

References

[1] M. Faustini, L. Nicole, E. Ruiz-Hitzky, C. Sanchez, *Adv. Funct. Mater.* **2018**, *28*, 1.
[2] J. H. Choi, H. Wang, S. J. Oh, T. Paik, P. S. Jo, J. Sung, X. Ye, T. Zhao, B. T. Diroll, C. B. Murray, C. R. Kagan, *Science* **2016**, *352*, 205.
[3] M. G. Ma, H. Cölfen, *Curr. Opin. Colloid Interface Sci.* **2014**, *19*, 56.
[4] M. P. Boneschanscher, W. H. Evers, J. J. Geuchies, T. Altantzis, B. Goris, F. T. Rabouw, S. A. P. P. Van Rossum, H. S. J. J. Van Der Zant, L. D. A. A. Siebbeles, G. Van Tendeloo, I. Swart, J. Hilhorst, A. V. Petukhov, S. Bals, D. Vanmaekelbergh, *Science* **2014**, *344*, 1377.

[5] J. J. De Yoreo, P. U. P. A. Gilbert, N. A. J. M. Sommerdijk, R. L. Penn, S. Whitelam, D. Joester, H. Zhang, J. D. Rimer, A. Navrotsky, J. F. Banfield, A. F. Wallace, F. M. Michel, F. C. Meldrum, H. Cölfen, P. M. Dove, *Science* **2015**, *349*.
[6] J. Zhang, Y. Li, X. Zhang, B. Yang, *Adv. Mater.* **2010**, *22*, 4249.
[7] S. Ni, L. Isa, H. Wolf, *Soft Matter* **2018**, *14*, 2978.
[8] N. Vogel, M. Retsch, C. A. Fustin, A. Del Campo, U. Jonas, *Chem. Rev.* **2015**, *115*, 6265.
[9] S. Sacanna, M. Korpics, K. Rodriguez, L. Colón-Meléndez, S.-H. Kim, D. J. Pine, G.-R. Yi, *Nat. Commun.* **2013**, *4*, 1688.
[10] M. V. Kovalenko, L. Manna, A. Cabot, Z. Hens, D. V. Talapin, C. R. Kagan, V. I. Klimov, A. L. Rogach, P. Reiss, D. J. Milliron, P. Guyot-Sionnnest, G. Konstantatos, W. J. Parak, T. Hyeon, B. A. Korgel, C. B. Murray, W. Heiss, *ACS Nano* **2015**, *9*, 1012.
[11] E. Bianchi, R. Blaak, C. N. Likos, *Phys. Chem. Chem. Phys.* **2011**, *13*, 6397.
[12] K. R. Phillips, G. T. England, S. Sunny, E. Shirman, T. Shirman, N. Vogel, J. Aizenberg, *Chem. Soc. Rev.* **2016**, *45*, 281.
[13] B. Sciacca, A. Berkhout, B. J. M. Brenny, S. Z. Oener, M. A. van Huis, A. Polman, E. C. Garnett, *Adv. Mater.* **2017**, *29*, 1.
[14] P. K. Kundu, D. Samanta, R. Leizrowice, B. Margulis, H. Zhao, M. Börner, T. Udayabhaskararao, D. Manna, R. Klajn, *Nat. Chem.* **2015**, *7*, 646.
[15] K. J. Dorsey, T. G. Pearson, E. Esposito, S. Russell, B. Bircan, Y. Han, M. Z. Miskin, D. A. Muller, I. Cohen, P. L. McEuen, *Adv. Mater.* **2019**, *31*, 1.
[16] M. J. Smith, C. H. Lin, S. Yu, V. V. Tsukruk, *Adv. Opt. Mater.* **2019**, *7*, 1.
[17] B. C. Steimle, J. L. Fenton, R. E. Schaak, *Science* **2020**, *367*, 418.
[18] B. J. Beberwyck, Y. Surendranath, A. P. Alivisatos, *J. Phys. Chem. C* **2013**, *117*, 19759.
[19] L. De Trizio, L. Manna, *Chem. Rev.* **2016**, *116*, 10852.
[20] J. M. Hodges, K. Kletetschka, J. L. Fenton, C. G. Read, R. E. Schaak, *Angew. Chemie - Int. Ed.* **2015**, *54*, 8669.
[21] T. Holtus, L. Helmbrecht, H. C. Hendrikse, I. Baglai, S. Meuret, G. W. P. Adhyaksa, E. C. Garnett, W. L. Noorduin, *Nat. Chem.* **2018**, *10*, 740.
[22] A. E. Powell, J. M. Hodges, R. E. Schaak, *J. Am. Chem. Soc.* **2016**, *138*, 471.
[23] C. D. Dieleman, W. Ding, L. Wu, N. Thakur, I. Bespalov, B. Daiber, Y. Ekinci, S. Castellanos, B. Ehrler, *Nanoscale* **2020**, *12*, 11306.
[24] K. Miszta, F. Greullet, S. Marras, M. Prato, A. Toma, M. Arciniegas, L. Manna, R. Krahne, *Nano Lett.* **2014**, *14*, 2116.
[25] R. J. Jackman, J. L. Wilbur, G. M. Whitesides, *Science* **1995**, *269*, 664.
[26] T. Kraus, L. Malaquin, H. Schmid, W. Riess, N. D. Spencer, H. Wolf, *Nat. Nanotechnol.* **2007**, *2*, 570.
[27] A. Perl, D. N. Reinhoudt, J. Huskens, *Adv. Mater.* **2009**, *21*, 2257.
[28] R. Klajn, M. Fialkowski, I. T. Bensemann, A. Bitner, C. J. Campbell, K. Bishop, S. Smoukov, B. A. Grzybowski, *Nat. Mater.* **2004**, *3*, 729.
[29] Q. A. Akkerman, G. Rainò, M. V. Kovalenko, L. Manna, *Nat. Mater.* **2018**, *17*, 394.
[30] S. D. Stranks, H. J. Snaith, *Nat. Nanotechnol.* **2015**, *10*, 391.
[31] M. A. Green, A. Ho-Baillie, *ACS Energy Lett.* **2017**, *2*, 822.
[32] W. Lee, J. Lee, H. Yun, J. Kim, J. Park, C. Choi, D. C. Kim, H. Seo, H. Lee, J. W. Yu, W. B. Lee, D. H. Kim, *Adv. Mater.* **2017**, *29*, 1.
[33] F. Zhang, H. Zhong, C. Chen, X. G. Wu, X. Hu, H. Huang, J. Han, B. Zou, Y. Dong, *ACS Nano* **2015**, *9*, 4533.
[34] J. Xue, Z. Zhu, X. Xu, Y. Gu, S. Wang, L. Xu, Y. Zou, J. Song, H. Zeng, Q. Chen, *Nano Lett.* **2018**, *18*, 7628.
[35] Y. Wei, Z. Cheng, J. Lin, *Chem. Soc. Rev.* **2019**, *48*, 310.
[36] H. Wei, Y. Fang, P. Mulligan, W. Chuirazzi, H. H. Fang, C. Wang, B. R. Ecker, Y. Gao, M. A. Loi, L. Cao, J. Huang, *Nat. Photonics* **2016**, *10*, 333.

[37] Q. Chen, J. Wu, X. Ou, B. Huang, J. Almutlaq, A. A. Zhumekenov, X. Guan, S. Han, L. Liang, Z. Yi, J. Li, X. Xie, Y. Wang, Y. Li, D. Fan, D. B. L. Teh, A. H. All, O. F. Mohammed, O. M. Bakr, T. Wu, M. Bettinelli, H. Yang, W. Huang, X. Liu, *Nature* **2018**, *561*, 88.
[38] C. H. Lin, Q. Zeng, E. Lafalce, S. Yu, M. J. Smith, Y. J. Yoon, Y. Chang, Y. Jiang, Z. Lin, Z. V. Vardeny, V. V. Tsukruk, *Adv. Opt. Mater.* **2018**, *6*, 1.
[39] C.-K. Lin, Q. Zhao, Y. Zhang, S. Cestellos-Blanco, Q. Kong, M. Lai, J. Kang, P. Yang, *ACS Nano* **2020**.
[40] M. E. Kamminga, H. H. Fang, M. A. Loi, G. H. Ten Brink, G. R. Blake, T. T. M. Palstra, J. E. Ten Elshof, *ACS Appl. Mater. Interfaces* **2018**, *10*, 12878.
[41] G. Wang, D. Li, H. C. Cheng, Y. Li, C. Y. Chen, A. Yin, Z. Zhao, Z. Lin, H. Wu, Q. He, M. Ding, Y. Liu, Y. Huang, X. Duan, *Sci. Adv.* **2015**, *1*, 1.
[42] B. H. Kim, M. S. Onses, J. Bin Lim, S. Nam, N. Oh, H. Kim, K. J. Yu, J. W. Lee, J. H. Kim, S. K. Kang, C. H. Lee, J. Lee, J. H. Shin, N. H. Kim, C. Leal, M. Shim, J. A. Rogers, *Nano Lett.* **2015**, *15*, 969.
[43] J. Chen, Y. Wu, X. Li, F. Cao, Y. Gu, K. Liu, X. Liu, Y. Dong, J. Ji, H. Zeng, *Adv. Mater. Technol.* **2017**, *2*, 1.
[44] C. Zhang, B. Wang, W. Li, S. Huang, L. Kong, Z. Li, L. Li, *Nat. Commun.* **2017**, *8*, 1138.
[45] H. Wang, R. Haroldson, B. Balachandran, A. Zakhidov, S. Sohal, J. Y. Chan, A. Zakhidov, W. Hu*, ACS Nano* **2016***, 10,* 10921.
[46] N. Pourdavoud, S. Wang, A. Mayer, T. Hu, Y. Chen, A. Marianovich, W. Kowalsky, R. Heiderhoff, H.-C. Scheer, T. Riedl, *Adv. Mater.* **2017***, 29,* 1605003.
[47] O. Bar-On, P. Brenner, U. Lemmer, J. Scheuer, *Adv. Mater. Technol.* **2018**, *3*, 1800212.
[48] F. Palazon, Q. A. Akkerman, M. Prato, L. Manna, *ACS Nano* **2016**, *10*, 1224.
[49] Y. C. Wong, W. Bin Wu, T. Wang, J. D. A. Ng, K. H. Khoo, J. Wu, Z. K. Tan, *Adv. Mater.* **2019**, *31*, 1.
[50] H. L. Clever, F. J. Johnston, *J. Phys. Chem. Ref. Data* **1980**, *9*, 751.
[51] A. A. Zhumekenov, M. I. Saidaminov, M. A. Haque, E. Alarousu, S. P. Sarmah, B. Murali, I. Dursun, X. H. Miao, A. L. Abdelhady, T. Wu, O. F. Mohammed, O. M. Bakr, *ACS Energy Lett.* **2016**, *1*, 32.
[52] L. Hong, J. Milic, P. Ahlawat, M. Mladenovic, D. J. Kubicki, F. Jahanbakhshi, D. Ren, M. Gelvez-Rueda, M. A. Ruiz-Preciado, A. Ummadisingu, Y. Liu, C. Tian, L. Pan, S. M. Zakeeruddin, A. Hagfeldt, F. C. Grozema, U. Rothlisberger, L. Emsley, H. Han, M. Grätzel, *Angew. Chemie Int. Ed.* **2019**.
[53] Y. T. H. Kim, G. H. Lee, Y. T. H. Kim, C. Wolf, H. J. Yun, W. Kwon, C. G. Park, T. W. Lee, *Nano Energy* **2017**, *38*, 51.
[54] H. Fang, W. Deng, X. Zhang, X. Xu, M. Zhang, J. Jie, X. Zhang, *Nano Res.* **2019**, *12*, 171.
[55] C. Cennini, G. Tambroni, *Di Cennino Cennini Trattato Della Pittura*, Paolo Salviucci, Rome, **1821**.
[56] W. Anaf, O. Schalm, K. Janssens, K. De Wael, *Dye. Pigment.* **2015**, *113*, 409.
[57] V. Rahemi, N. Sarmadian, W. Anaf, K. Janssens, D. Lamoen, B. Partoens, K. De Wael, *Anal. Chem.* **2017**, *89*, 3326.
[58] I. Fiedler, M. a. Bayard, in *Artist. - A Handb. Their Hist. Charact.* (Ed.: R.L. Feller), National Gallery Of Art, Washington, **1986**, pp. 104–105.
[59] M. Eder, S. Amini, P. Fratzl, *Science* **2018**, *362*, 543.
[60] M. R. Begley, D. S. Gianola, T. R. Ray, *Science* **2019**, *364*.
[61] F. L. Bargardi, H. Le Ferrand, R. Libanori, A. R. Studart, *Nat. Commun.* **2016**, *7*, 1.
[62] http://creativecommons.org/licenses/by/4.0.
[63] https://wellcomecollection.org/works/s7fye3z3.

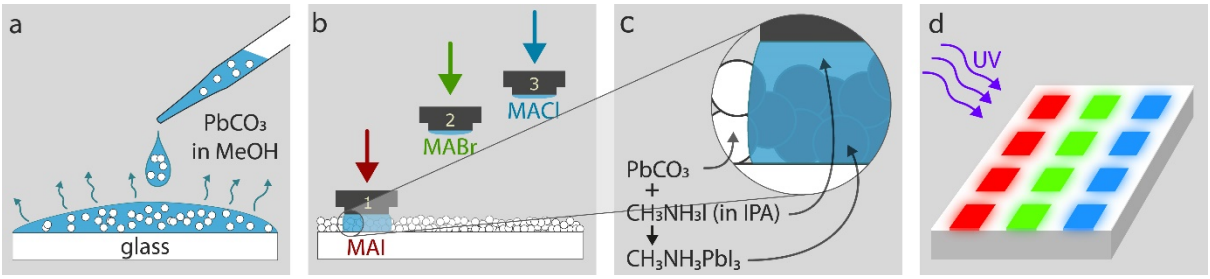

Figure 1. Schematic illustration showing the fabrication of a spatially patterned perovskite film. a) Drop casting $PbCO_3$ particles dispersed in methanol onto a glass substrate results in a $PbCO_3$ thin film that acts as the reactive canvas. b) Stamping MAX in IPA on the canvas results in, c) spatially-controlled conversion of the $PbCO_3$ into a $MAPbX_3$ perovskite. d) Upon UV irradiation, the converted areas emit light with a color that is controlled by adjusting the halide moiety of the perovskite.

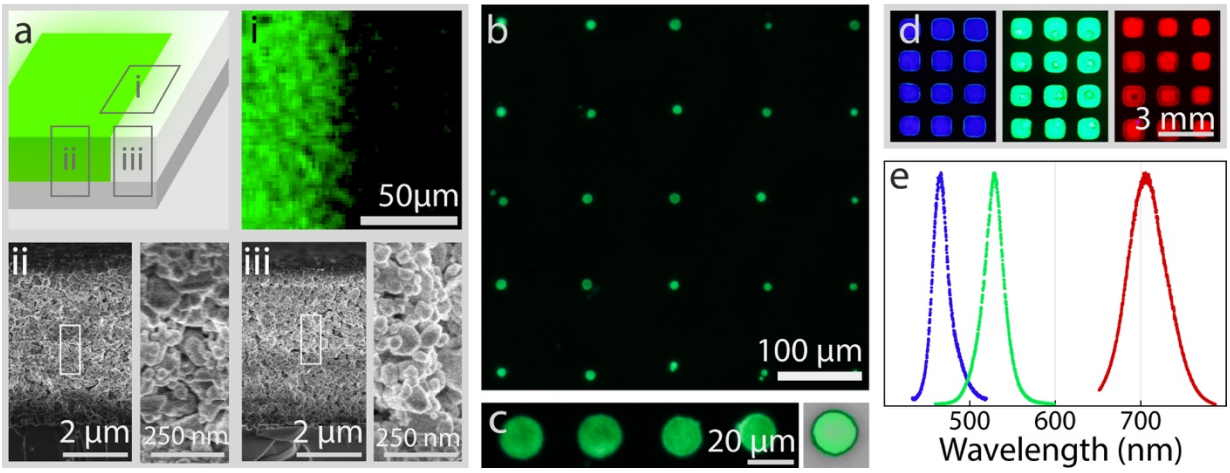

Figure 2. Characterization of contact printed perovskite pixels. a) Schematic overview of a printed pixel: i) EDS elemental mapping of Br atoms, ii) cross-section of a converted film with close-up (SEM), iii) cross-section of a pristine film with close-up (SEM). b) Photoluminescence microscopy image of a square array of contact printed dots spaced 100 µm apart. c) Photoluminescence microscopy image of: (left) array of 20 µm dots spaced 40 µm, (right) 20 µm PDMS stamp overlayed with the resulting photoluminescence dot pattern. d) Fluorescence photographs of contact-printed perovskite pixels of different emission colors by tuning the

halide moiety: left to right: MACl-MABr (6:4), MABr, MABr-MAI (2:8). e) Corresponding normalized photoluminescence spectra of the perovskites shown in Figure 2d.

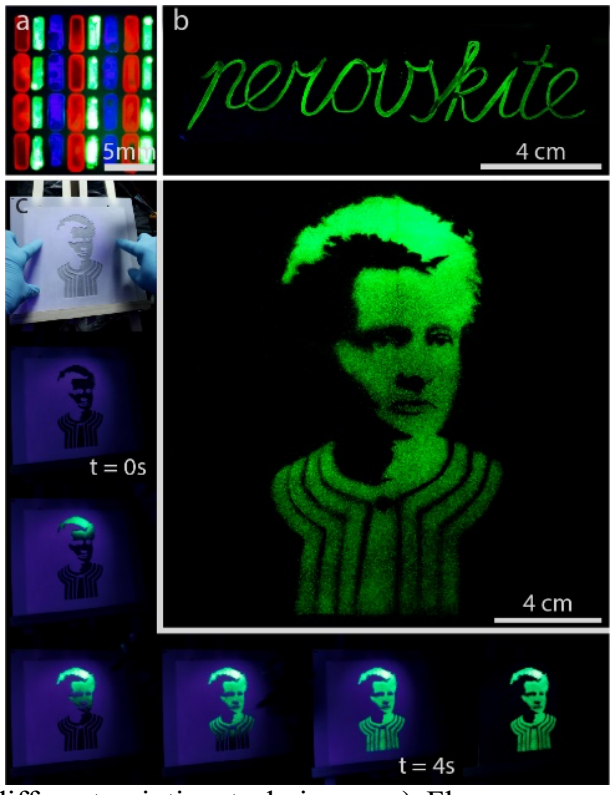

Figure 3. IEL via different printing techniques. a) Fluorescence photograph of multicolor contact printed pixels: FABr-FAI (2:8) (red), MABr (green), and MACl-MABr (6:4) (blue) separated by unconverted $PbCO_3$. b) Fluorescence photograph of a pattern drawn by applying the conversion ink with a paintbrush. c) Time-lapse of an airbrush painting of Marie Skłodowska-Curie: a 20x20 cm film of $PbCO_3$ is selectively shielded with a stencil (the polymer in the stencil fluoresces blue under UV irradiation), MABr/IPA is applied with an airbrush gun, the ion exchange reaction creates perovskite that luminesces green under UV irradiation, removal of the stencil shows the portrait. (d) Reproduced under the terms of the CC-BY Creative Commons Attribution 4.0 International license.[62] Copyright: Wellcome Collection [Portrait of Marie Skłodowska Curie (1867 – 1934), Polish-French physicist and chemist, Nobel Laureate in physics (1903) and chemistry (1911)].[63]

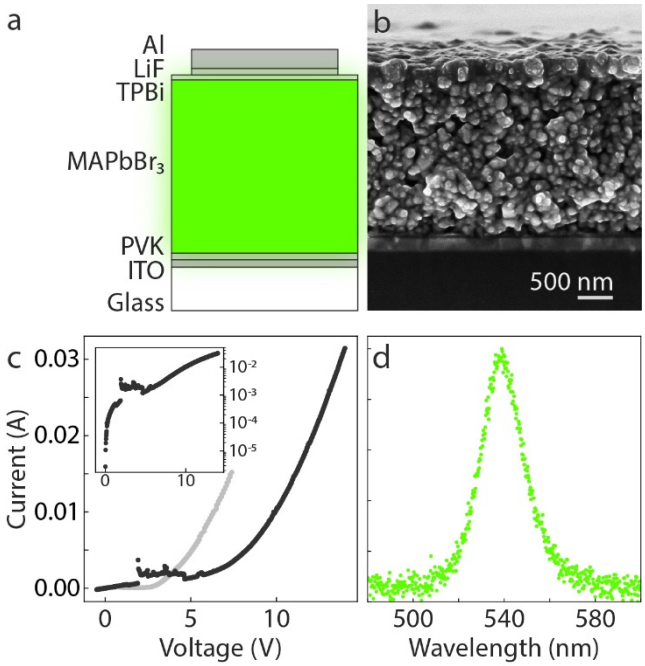

Figure 4. LED based on IEL. a) Schematic of the layers used in this LED, b) Cross section of a device imaged by SEM. c) IV measurement of an IEL-based LED (black, inset logarithmic scale) and a conventional led (grey), and d) normalized EL showing green light emission of the LED at 10 V.

This work introduces Ion Exchange Lithography (IEL) for integrating user-defined patterns of desirable chemical compositions in thin films. In IEL, a reactive nanoparticle "canvas" is locally converted by printing ion exchange "inks". The proof-of-concept and versatility are demonstrated by printing, painting, and airbrushing inks to create perovskite semiconductors with tunable composition. The functional potential is explored by fabricating a light-emitting diode.

*L. H., M. H. F., L. A. M., B. E., W. L. N.**

Ion Exchange Lithography: Localized Ion Exchange Reactions for Spatial Patterning of Perovskite Semiconductors and Insulators

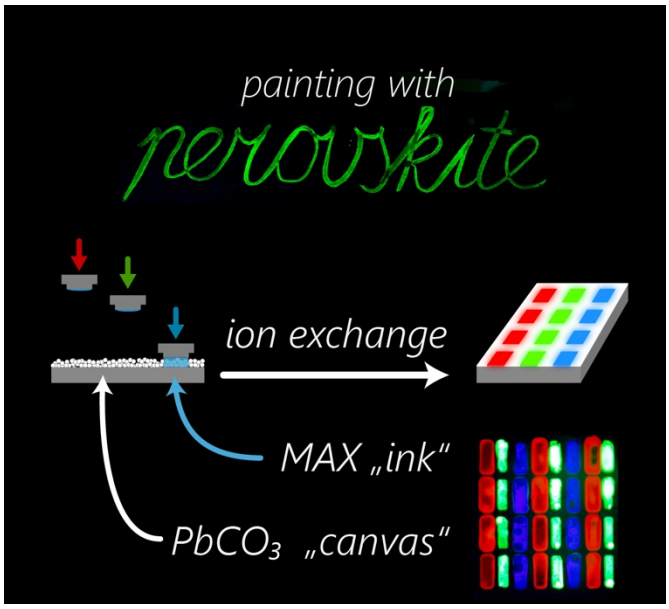

Supporting Information

Ion Exchange Lithography: Localized Ion Exchange Reactions for Spatial Patterning of Perovskite Semiconductors and Insulators

*Lukas Helmbrecht, Moritz H. Futscher, Loreta A. Muscarella, Bruno Ehrler, Wim L. Noorduin**

Fabrication of lead-carbonate canvas

Lead carbonate powder (2 g, Alfa Aesar, lead(II)carbonate, ACS, 40119) was dispersed in 10 ml isopropyl alcohol with glass beads in a 20 ml vial, and ground for ten consecutive days in an ultrasonic bath (VWR Ultrasonic Cleaner USC-THD). Subsequently, the nanocrystalline lead carbonate powder was isolated from the slurry by filtration.

To prepare the canvas, the nanocrystals were dispersed in methanol (25 mg $PbCO_3$/ml MeOH) and sonicated for 180 minutes at room temperature. Microscope slides were cut to 15x15 or 17x17 mm squares, cleaned with isopropyl alcohol, and plasma cleaned for 10 minutes. Typically, 150-200 µL of the $PbCO_3$/MEOH was drop casted onto each substrate. To obtain the canvas, the solvent was left to evaporate at 45°C in an oven. Thinner films were achieved by diluting the dispersion (Figure S1). The lead carbonate canvas used for the airbrushed portrait and the "perovskite" lettering was obtained by covering a 20x20 cm ceramic tile with double-sided tape and brushing lead carbonate onto it (see also Figure S2g).

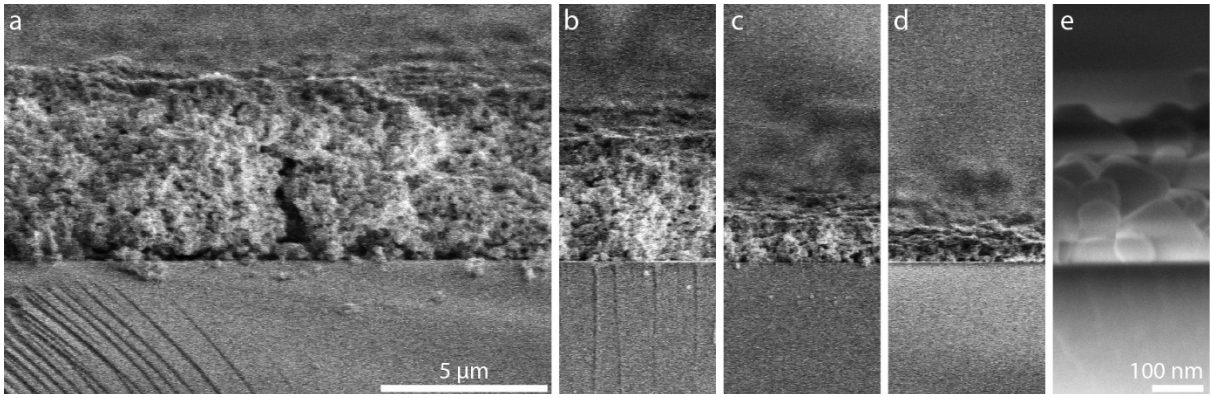

Figure S1. Lead carbonate nanoparticle films of decreasing thickness. a) 5µm film created with stock solution. b-e) Dilution of the dispersion allows for thinner films. Note the higher magnification in e).

Stamps were prepared from commercially available silicone (Zhermack elite double, 32 shore). The silicone is available in a variety of degrees of hardness. We find that softer stamps damage the film, whereas harder stamps fail to make uniform contact. The stamps were fabricated by casting the liquid silicone into 3D printed molds. We designed patterns with 1x1 mm studs and 1 mm spacing, as well as a pattern of 1.5x3 mm studs. The later pattern was split into three parts on three stamps for sequential application (Figure S2).

The conversion ink was prepared by dissolving 0.16 mmol methyl ammonium or formamidinium halide per mL isopropyl alcohol under inert environment. The crucial parameters for successful stamping are the amount of ink that is transferred and the applied

pressure. To control the amount of liquid, 25 µl conversion ink is placed in a petri dish. A 20x20 mm piece of foam board is pressed onto that drop. The stamp is inked by gently pressing it against the foam board. To contact print the $PbCO_3$, the stamp is gently pressed on the canvas, assuring sufficient contact pressure to transfer the ink without damaging the canvas.

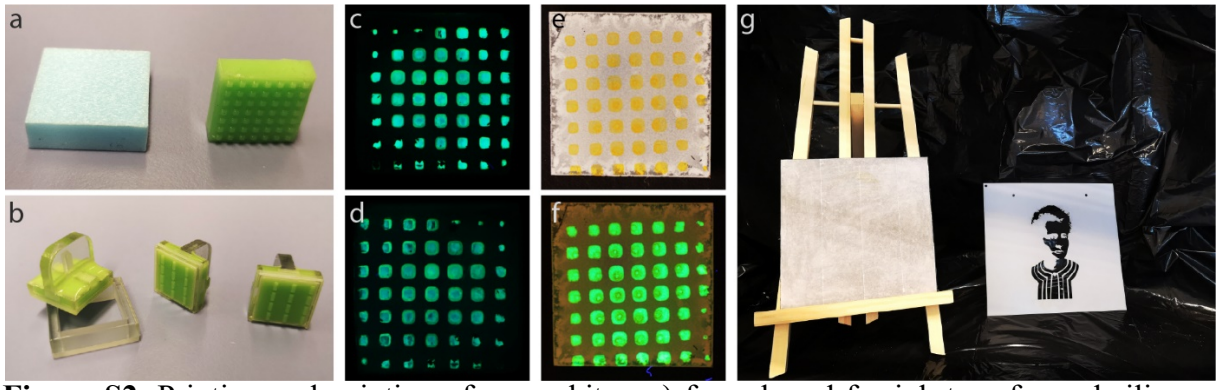

Figure S2. Printing and painting of perovskites. a) foam board for ink transfer and silicone stamp. b) silicone stamps with guiding frame to integrate different compositions, c) and d) perovskite pattern on glass, imaged from the front and backside, respectively, showing conversion throughout the film. f) and g) perovskite pattern in daylight and with additional UV light, respectively. c) Setup for airbrush painting with a stencil.

IEL with micropatterned PDMS stamps

Poly(dimethyl)silane (PDMS) stamps with micropatterns were cast from SU8-Si masters using replica molding. The SU8-Si masters were prepared using standard photolithography methods. Subsequently, the surface of the SU8-Si master, containing a negative of the desired pattern, was chemically modified with silane groups. To this aim, the SU8-Si master was placed in a desiccator with two drops of a fluoroalkylsilane and put under reduced pressure for minimal 2 hours. Subsequently, the stamp was fabricated by casting poly(dimethyl)silane (Sylgard 184) on the silanized master. After curing at 65 °C for 2 hours, the PDMS stamp was carefully peeled off the master.

Ion exchange ink was carefully applied in the same manner as for the silicon stamps. The stamp was then first brought in contact with a sacrificial $PbCO_3$ film to “pre-stamp” and remove excess ink before pressing it onto the lead carbonate canvas.

Characterization of perovskite samples

The fluorescent nature of the perovskites is a convenient first indicator of successful conversions. Illuminated with a UV LED (365 nm), the converted parts light up. The photographs in Figures 2 and 3 were taken with a Canon 800D camera equipped with a Sigma 17-70 mm macro lens and a UV filter.

Scanning electron microscopy micrographs were captured with an FEI Verios 460. The EDS (energy dispersive X-Ray spectroscopy) map of bromide distribution was recorded with an additional Oxford X-Max^n energy dispersive X-ray spectrometer (Figure 2 and S3).

Photoluminescence was studied using a Witec alpha 300 in combination with a Thorlabs S1FC405 405nm laser.

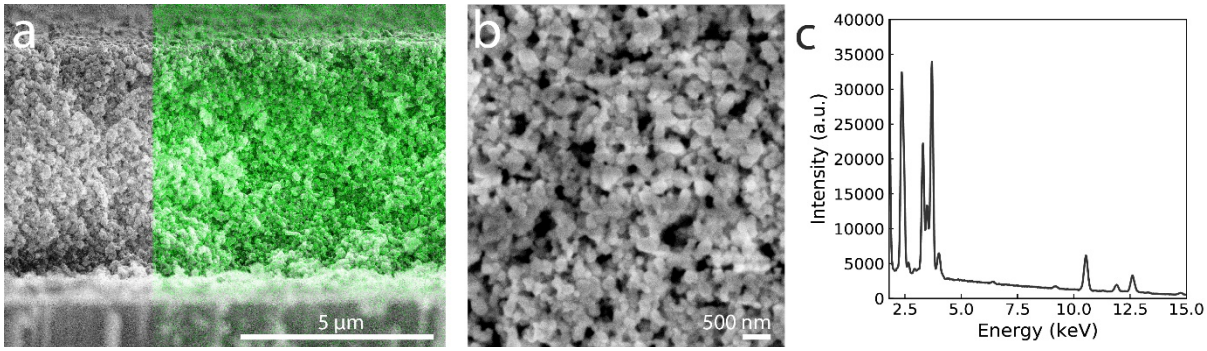

Figure S3. a) EDS map of a cross-sectioned, converted canvas. Left: SEM image showing the nanoparticles in the film. Right: Elemental map overlay showing the presence of bromide (green) throughout the film, indicating conversion from top to bottom. b) High resolution SEM image showing the morphology retention in a $PbCO_3$ film exposed to FABr for 30 minutes. b) EDS spectrum of this film, showing the characteristic peaks of the glass substrate, lead, and bromide, allowing an analysis of the composition (25/75 at.% (Br/Pb)).

LED fabrication

The stack used to fabricate the LED is ITO/PVK/ perovskite/TPBi/LiF/Al. First, glass-ITO substrates were cleaned with sonication subsequently for 15 minutes in detergent in deionized water, acetone, and isopropanol, followed by oxygen plasma for 15 minutes at 100 W. The hole injection layer is prepared by dissolving 9 mg of Poly(9-vinylcarbazole) powder in 1 mL of chlorobenzene, stirred overnight and then spun at 2000 rpm for 60 seconds with a ramp of 1000 rpm/s on the cleaned ITO substrates. The films were then annealed at 120 °C for 20 minutes.

Second, the $PbCO_3$ canvas was created and converted to perovskite: after 1 second of plasma cleaning of the PVK surface, 150 µl of $PbCO_3$ dispersion (prepared as above, settled for 24h) were drop cast onto the PVK film at 50°C. The lead carbonate films were converted to perovskite by immersing them into a conversion ink for 30 seconds (0.16 mmol/ml FABr in anhydrous IPA) and drying them under N_2 flow.

Finally, the films were taken into an evaporation chamber where 40 nm TPBi (0.1 Å/s), 1.2 nm LiF (0.1 Å/s), and 100 nm Al (1 Å/s) were sequentially deposited at a pressure of 10^{-7} mbar to serve as electron injection layer and cathode. Prior IV and EL characterizations, the devices were encapsulated using epoxy glue and glass coverslips.

Photoluminescence Quantum Yield

We characterize the photoluminescence quantum yield (PLQY) of the ion exchanged films with a custom-built setup. The details have been previously published (B. K. Patra *et al.* ACS Applied Materials & Interfaces 2020, 12, 31764). It is based on a Labsphere integrating sphere. The sample is placed inside the sphere and excited with a UV laser (Thorlabs, L405P20, 405 nm) which is modulated by optical chopper (Thorlabs, MC2000B-EC). Light leaving the integrating sphere is collected with a low-noise calibrated photodetector (Newport 818-SL) which is read out by an lock-in amplifier (Stanford Research Systems SR830) lock-in amplifier. The excitation and emission are measured separately, using a short pass filter (Thorlabs FESH0450) and long pass filter (Thorlabs FELH0450) in front of the photodetector, respectively. The PLQY (η) is calculated as follows:

$$\eta = \frac{P_c - (1-A)P_b}{L_a A} \quad \text{, with} \quad A = \frac{L_b - L_c}{L_b} = 1 - \frac{L_c}{L_b} \,. \qquad (1)$$

P_c and P_b are the photoluminescence resulting from direct and indirect excitation of the sample. L_a, L_b, and L_c are the laser light intensity, leaving the sphere, measured for an empty sphere, indirect excitation, and direct excitation of the sample, respectively. A is the absorbance of the sample.

LED characterization

The top contact, as well as the ITO film, was segmented into six sections, which could be individually addressed. A custom software took care of recording the current density versus voltage behavior via a Keithley 2440. For the EL measurement, a continuous voltage of 10 V was applied while simultaneously capturing the emitted light with a fiber-coupled spectrometer (Ocean Optics). To enhance the light collection, a 30 mm lens was mounted above the device to collect the emission and focus it into the fiber towards the spectrometer.

Photoluminescence of Formamidinium Lead Halide Perovskites

Formamidinium lead halide perovskites can be created via ion exchange of $PbCO_3$ with formamidinium halide inks. Figure 7 shows typical PL spectra of blue-, green-, and red-emitting perovskites.

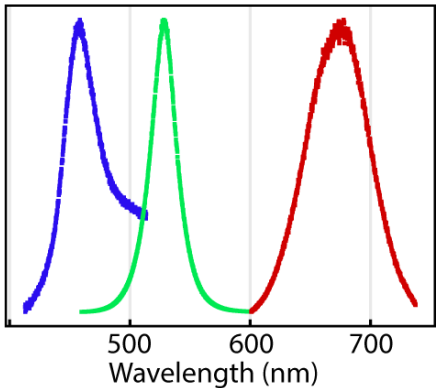

Figure S4. Normalized photoluminescence spectra of formamidinium lead halide perovskites created by ion exchange reaction of $PbCO_3$ with: blue: FACl-FABr (6:4); green: FABr, red: FABr-FAI (2:8).

IR spectroscopy analysis

We performed IR-spectroscopy studies on $PbCO_3$ films before and after conversion to $MAPbBr_3$ using a Bruker Vertex 80v FT-IR spectrometer. For these experiments, we deposited a thin film (0.5-1.0 µm) of $PbCO_3$ nanoparticles on IR-transparent calcium fluoride substrates and measured under nitrogen atmosphere. The partially converted sample shows characteristic perovskite peaks (N-H stretch at 3200-3000 cm^{-1}, and -CH_3 rocking at 920 cm^{-1}) (Figure S5). However, no characteristic peaks of the expected side products H_2O (1650 cm^{-1}) and CH_3NH_2 (2900 cm^{-1}), and the solvent IPA (2950 cm^{-1}) are found.

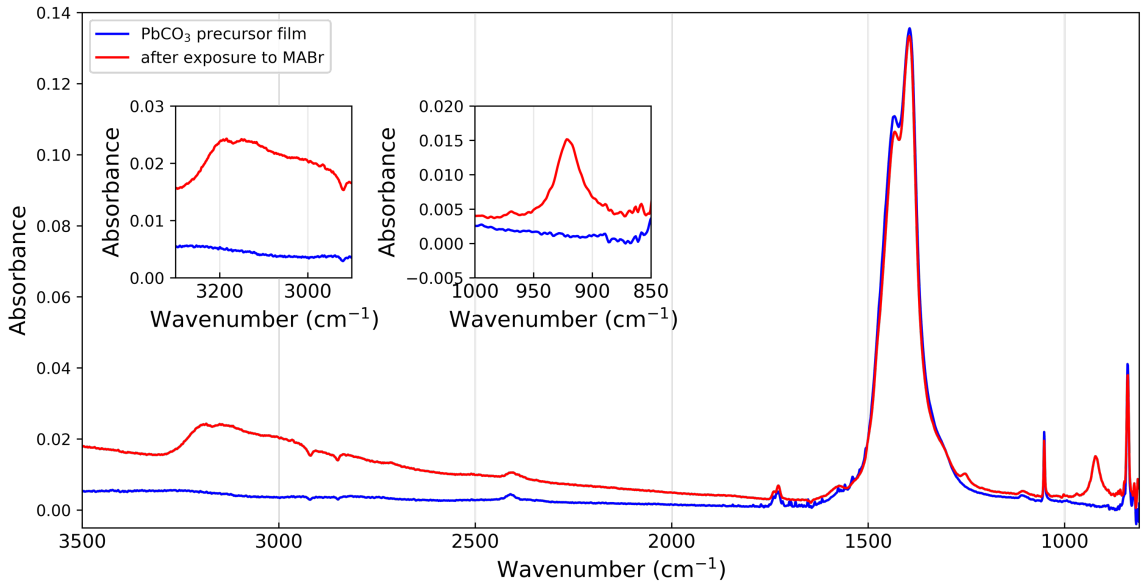

Figure S5. IR microscopy study of $PbCO_3$ film before and after partial conversion to $MAPbBr_3$, insets show characteristic perovskite peaks: N-H stretch at 3200-3000 cm^{-1}, and -CH_3 rocking at 920 cm^{-1}. The characteristic CO_3 peaks of $PbCO_3$ at 1500-1300 cm^{-1} overlap with the C-H bend of the perovskite.